Reaction rates of hydroxyl radical with nitric acid and with hydrogen peroxide

William J. Marinelli and Harold S. Johnston

Citation: The Journal of Chemical Physics **77**, 1225 (1982); doi: 10.1063/1.443998
View online: http://dx.doi.org/10.1063/1.443998
View Table of Contents: http://scitation.aip.org/content/aip/journal/jcp/77/3?ver=pdfcov
Published by the AIP Publishing

Reaction rates of hydroxyl radical with nitric acid and with hydrogen peroxide[a)]

William J. Marinelli[b)] and Harold S. Johnston

Department of Chemistry, University of California and Materials and Molecular Research Division, Lawrence Berkeley Laboratory, Berkeley, California 94720
(Received 25 February 1982; accepted 12 April 1982)

The rates of the reactions $HO + HNO_3 \rightarrow H_2O + NO_3$, (1), $HO + H_2O_2 \rightarrow H_2O + HOO$ (2) have been studied by laser flash photolysis of reactants and resonance fluorescence of hydroxyl radicals. The recently reported high rate constants at room temperature for both reactions and the negative activation energy for Reaction (1) at low temperature have been confirmed. Results obtained here are: $k_1 = 1.52\times10^{-14}\exp(644/T)$ cm^3 molecule^{-1} s^{-1} from 218–363 K and $k_2 = 1.81\times10^{-12}$ cm^3 molecule^{-1} s^{-1} at 298 K. These two reactions have been examined by transition-state theory; (1) is assigned a cyclic and (2) a chainlike transition state. Even with no potential energy barrier, the reaction coordinate of (1) involves a quantum-mechanical, temperature independent frequency; and with this model the low pre-exponential factor and negative activation energy of Reaction (1) can be explained.

INTRODUCTION

Two recent measurements[1,2] of the rate coefficients for the reaction

$$HO + HNO_3 \rightarrow H_2O + NO_3 \qquad (1)$$

differ substantially from other measurements,[3–6] both as to value at 298 K and as to temperature dependence. Wine *et al.*[1] found the second-order rate coefficient for Eq. (1) to be

$$k_1 = 1.52\times10^{-14}\exp(649/T)\,\text{cm}^3\,\text{molecule}^{-1}\,\text{s}^{-1}$$

over the temperature range 224–366 K. The reaction has a "negative activation energy," i.e., the rate coefficient increases with a decrease in temperature.[1,2] The pre-exponential factor is about 10^{-14} cm^3 molecule^{-1} s^{-1}, which appears to be low for a hydrogen–atom transfer reaction. It has been established that NO_3 is the primary product of this reaction.[6,7]

Also, recent measurements[8–11] find the rate coefficient for the reaction

$$HO + H_2O_2 \rightarrow H_2O + HOO \qquad (2)$$

to be faster than that indicated by earlier studies.[12–14] For example, Keyser[8] found the rate expression

$$k_2 = 2.15\times10^{-12}\exp(-126/T)\,\text{cm}^3\,\text{molecule}^{-1}\,\text{s}^{-1}$$

over the temperature range 245–423 K. The activation energy is of small magnitude but it has the usual sign, and the pre-exponential factor is within the range regarded as "normal."

Since recent measurements of the rate constants for Reactions (1) and (2) differ substantially from the body of older data, it is desirable to reinvestigate these reactions in several different laboratories. In the present study the technique of laser flash photolysis coupled with product detection by resonance fluorescence (FP/RF) was used to study Reaction (1) from 218 to 363 K and to study Reaction (2) at 298 K.

The ratio of pre-exponential factors for these two apparently similar reactions is 165, and the ratio of rate coefficients k_2/k_1 is 12 at room temperature. In view of the low pre-exponential factor for k_1, the negative activation energy for Eq. (1), and the large ratio k_2/k_1 a complex mechanism such as

$$HO + HNO_3 \underset{M}{\overset{M}{\rightleftharpoons}} HO\cdot HNO_3 \xrightarrow{M} H_2O + NO_3 \qquad (3)$$

has been postulated where all steps presumably depend on foreign gas concentration. However, this study includes an examination of Reactions (1) and (2) by simple activated complex theory,[15] in order to see if each of these reactions could be an elementary bimolecular reaction within the framework of this theory and with the values of k_1 and k_2 that have been recently obtained.

EXPERIMENTAL

The apparatus used in these experiments is shown in Fig. 1. Two photolysis cells were employed. The first, designed after Magnotta,[16] was used for early experiments at 298 K. Later temperature-dependence experiments were performed in the cell shown in Fig. 2, similar to one described by Wine, Kreutter, and Ravishankara.[17] The jacketed Pyrex cell was externally blackened to reduce scattered light, wrapped with aluminum foil to minimize radiative heat exchange, and enclosed in a vacuum housing pumped to 10 μ for insulation. Methanol (218–273 K) or ethylene glycol (273–363 K) from a circulating temperature bath was passed through the cell jacket for temperature control. A temperature sensor, which could be inserted into the reaction zone, determined the gas temperature to ± 1 K. Two Suprasil-1 lenses were used weakly to focus light from the resonance lamp into the reaction zone and to collect resonantly scattered radiation for focusing on to the PMT detector. All window materials were Suprasil-1 or CaF_2.

The resonance lamp used for HO radical resonance

[a)]This work was supported by the Director, Office of Energy Research, Office of Basic Energy Sciences, Chemical Sciences Division of the U. S. Department of Energy under Contract No. DE-AC03-76SF00098.
[b)]Present address: Department of Chemistry, Cornell University, Ithaca, New York 14853.

 0021-9606/82/151225-10$02.10

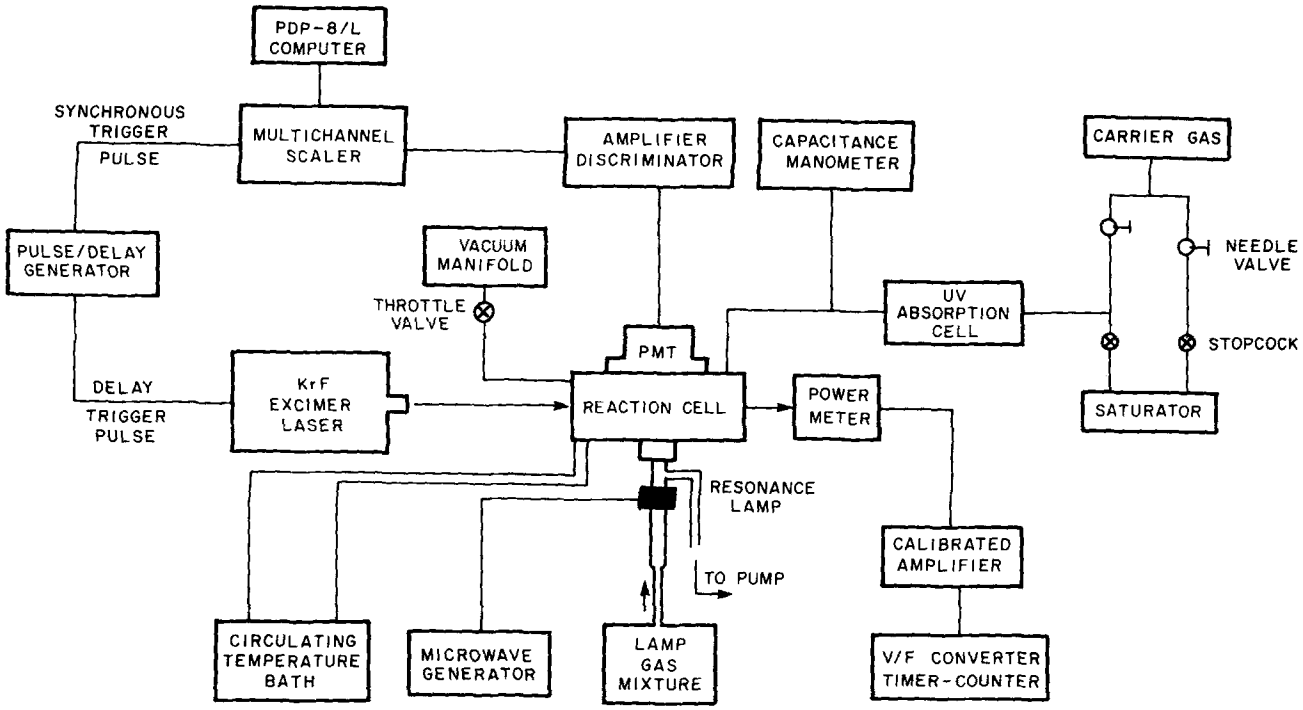

FIG. 1. Schematic diagram of FP/RF apparatus. Resonance lamp is shown on PMT axis but actually is perpendicular.

fluorescence detection was operated with a 3% H_2O/Ar mixture at ~ 700 μ total pressure, and used a 2.45 GHz current stabilized microwave generator. Vycor was used as a lamp window to eliminate unwanted UV and VUV radiation emitted from the lamp. The detection system consisted of a cooled RCA 31034 PMT and a baffled Hoya "Peak 320" color filter and 307 ± 15 nm interference filter. These filters passed the HO ($A\,^2\Sigma^+ - X\,^2\pi_i$) (0, 0) band while rejecting scattered photolysis laser light. Response of the detection system was shown to be linear from $0.5-5\times10^{11}$ molecules/cm^3 with a sensitivity of 3×10^7 molecules cm^{-1} Hz^{-1} by photolysis of a fixed HNO_3/Ar mixture at varying energies.

Hydroxyl radicals were produced by photolysis of the reactant molecules HNO_3 or H_2O_2. A Lumonics TE-860-2M rare gas halide excimer laser running on KrF at 248.4 nm and operated at 15 Hz with typical pulse energies of 10–20 mJ/cm^2 was used. Average laser power was measured using a Scientech surface absorbing power meter.

Concentrations of reactants were measured continuously using a UV absorption system. It consisted of a 1 m long Pyrex cell, equipped with fused silica windows, through which the chopped output of a Beckman deuterium lamp was directed. Light emerging from the cell passed through a (McPherson 218) 0.3 m monochrometer set at 0.3 nm bandpass and was detected by an RCA 1P28 photomultiplier coupled to a lock-in amplifier. The monitoring cell was run at ambient temperature. Readings from a second temperature sensor fixed to the cell were used to correct reactant concentrations for changes in gas density between the monitoring and photolysis cell due to temperature differences. Nitric acid and H_2O_2 were monitored at 200 nm using the absorption cross sections of Molina and Molina[18]: $\sigma_{HNO_3} = 6.6\times10^{-18}$ cm^2 molecule^{-1} and $\sigma_{H_2O_2} = 4.67\times10^{-19}$ cm^2 molecule^{-1}. Reactants were introduced into the system via partial saturation of Ar carrier gas passed through a Pyrex saturator held at 232 or 244 K (HNO_3) or 273 K (H_2O_2). Fine control of reactant concentrations was accomplished using a split-flow system employing two Nupro-type "s" stainless steel needle valves placed in the carrier gas lines before the saturator. The saturator was equipped with by-pass valves which allowed only pure carrier gas to flow through the system and enabled the determination of the UV cell 100% transmission level. A short length of large diameter (1/2 in.) tubing was used to connect the photolysis and monitoring cells, and a throttle valve was used to limit the pump-out rate of the system. Two cross calibrated capacitance manometers placed at each end of the flow system showed less than a 1% pressure drop under flowing experimental conditions of 100 sccm Ar at 10 Torr total pressure. At higher pressures, a constant cell residence time was maintained by adjusting the flow rate and pump throttle valve. Under these conditions, reactant concentrations were stable to within 3% after a 10 min. (600 residence times) equilibration period.

The PMT was operated in photon counting mode using a PAR 1121 amplifier/discriminator coupled to an SSR 1105 photon counter with an ECL/TTL converter and high speed line driver. Data were recorded using a Nicolet Instruments (Fabritek) 1074 instrument computer acting as a signal averager in multichannel scaling mode and analyzed using a PDP-8/L computer interfaced to the signal averager. Typically, 1024 channel segments at channel widths of 2–20 μs were used and 4096 or 8192 laser shots were averaged to obtain a first-order rate constant.

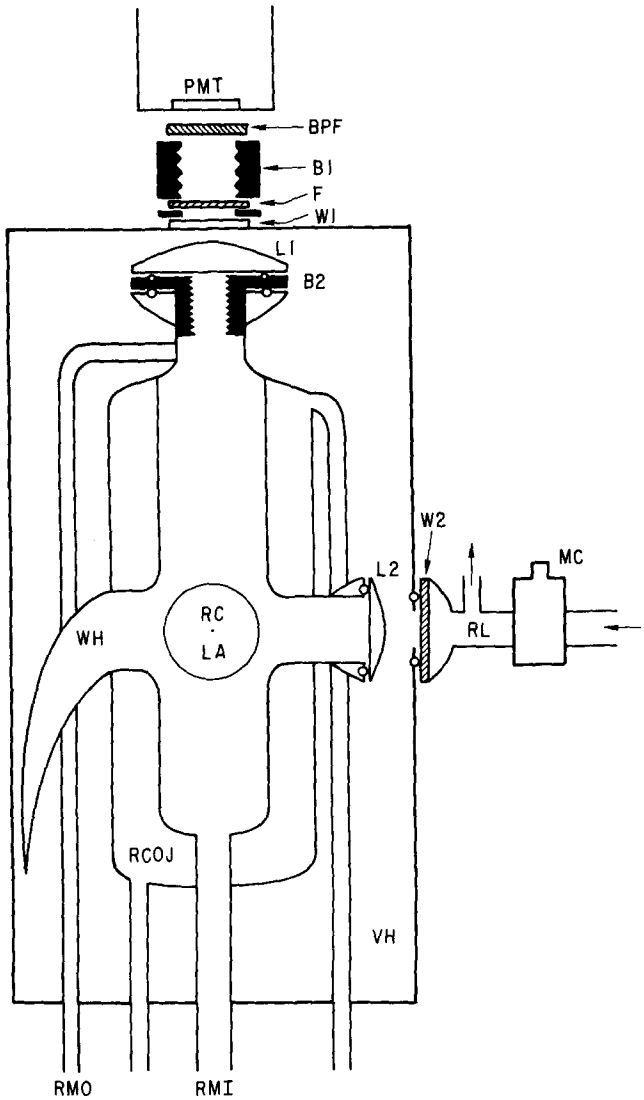

FIG. 2. Schematic diagram of reaction cell, resonance lamp, and detector geometries. PMT RCA 31034 photomultiplier tube, BRP 309 nm interference filter, $B1$ and $B2$ scattered light baffles, F Hoya "Peak 320" color filter, $W1$ CaF_2 window, $L1$ 1–1/2 in. diameter × 2 in. f.l. Suprasil-1 lense, $L2$ 1 in. diameter × 1–12 in. f.l. Surpasil-1 lense, $W2$ Vycor resonance lamp window, RL resonance lamp, MC microwave cavity, WH, woods horn, LA photolysis laser axis, RC reaction cell interaction region, RCOJ reaction cell temperature control outer jacket, VH vacuum housing, RMI reaction mixture in, RMO reaction mixture pump out.

MATERIALS

The Ar (> 99.999%) and N_2 (> 99.998%) were supplied by Lawrence Berkeley Laboratory and used without further purification. Nitric acid was prepared by distillation from mixtures of $NaNO_3$ or KNO_3 in excess 96% H_2SO_4 under vacuum. The product was collected at 244 K (*o*-xylene slush) from a distillation flask held at 300 K with only the middle portion saved, and it was stored at 196 K. The concentration of NO_2 in the HNO_3 samples was always less than the detection limit of 0.05%. Hydrogen peroxide was purchased as a 90% or 98% solution from FMC Corporation and was degassed by pumping prior to use.

RESULTS

The reaction of HO with HNO_3

The FP/RF experiments were conducted under pseudofirst-order conditions with reactant concentrations 10^2–10^4 times greater than HO following the flash. The reaction of HO with HNO_3 was studied over a 23-fold range of HNO_3 concentration, a fivefold range of Ar carrier gas pressure from 10 to 50 Torr, and a 145 K temperature range from 218–363 K. The HO radical decays were analyzed using standard first-order techniques

$$\ln F_t = \ln F_0 - k't \,, \tag{4}$$

where F is the observed fluorescence signal which is proportional to the hydroxyl radical concentration

$$F = \alpha[\mathrm{HO}] \,, \tag{5}$$

so that Eq. (4) is equivalent to

$$\ln[\mathrm{HO}]_t = \ln[\mathrm{HO}]_0 - k't \,. \tag{6}$$

The pseudofirst-order constant k' is determined by a least-squares analysis of Eqs. (4) or (6), and it has the property

$$k' = k_1[\mathrm{HNO_3}] + k_d \,. \tag{7}$$

The second-order rate constant of interest k_1 is obtained from the slope of a plot of k' vs $[HNO_3]$. The intercept gives k_d, which is a first-order rate constant describing HO removal processes not proportional to the concentration of reactant, such as diffusion, reaction with carrier gas or impurities, and flow. In the HNO_3 study, corrections were considered for the competing reaction

$$\mathrm{HO} + \mathrm{NO_2} \xrightarrow{\mathrm{M}} \mathrm{HNO_3} \,. \tag{8}$$

The ratio of the rate of Eq. (8) to that of Eq. (1) is $k_8^0[\mathrm{M}][\mathrm{NO_2}]/k_1[\mathrm{HNO_3}]$, where k_8^0 is the low-pressure limit $2.6\times10^{-30}\,(300/T)^5$. In all cases, the ratio $[NO_2]/[HNO_3]$ was below the detection limit of 5×10^{-4}, and the maximum pressure was 50 Torr at room temperature and 25 Torr at other temperatures. The upper limit to the correction for Eq. (8) is 2% at 218 K, 1.5% at 300 K, and 0.5% at 363 K. Decays were typically followed for 1.5 to 3 hydroxyl radical lifetimes ($1/e$) with a return to baseline during the sweep in all but the lowest reactant concentration experiments. A typical HO radical decay is shown in Fig. 3 along with the least-squares fit to the data.

The pseudofirst-order rate constants k' are plotted against the concentration of HNO_3 at 298 K for 10, 25, and 50 Torr of argon carrier gas in Fig. 4. The three lines are parallel to each other giving the same second-order rate coefficient k_1. The intercepts are in the order one would expect from diffusion as the dominant effect in k_d: the largest k_d is with 10 Torr carrier gas, the intermediate value is with 25 Torr, and the smallest value of k_d is with 50 Torr. In the recent work by Nelson *et al.*,[6] the relation of k_d to carrier gas pressure was in the inverse order, and one value of k_d appeared to be unusually high. The current study involved many more rate-constant determinations, and the present results are regarded as more reliable than those of

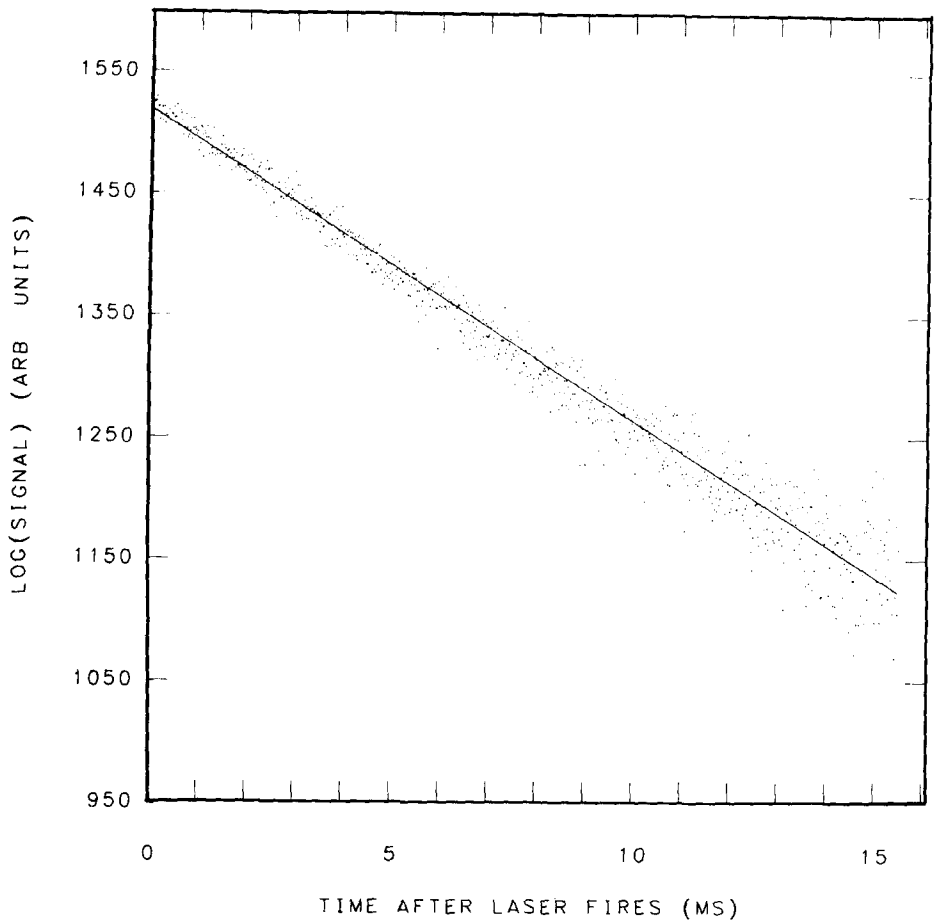

FIG. 3. An example of HO decay in nitric acid [compare Eq. (4)]. Dots experimental data, solid line least-squares fit, which starts 1 ms after laser fires. The slope gives pseudo-first-order rate constant [Eq. (7)].

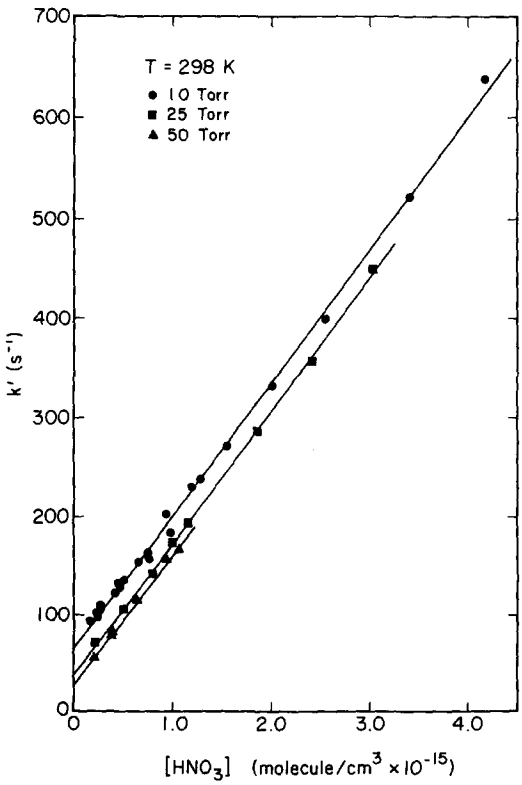

FIG. 4. Plot of pseudofirst-order rate constants against $[HNO_3]$ for the reaction of HO with HNO_3. The slopes give the second-order rate constants $k_1 = (1.35, 1.35, 1.33) \times 10^{-13}$ cm^3 $molecule^{-1}$ s^{-1}, at 10, 25, and 50 Torr, respectively.

Nelson *et al.*[6] on this reaction. In addition, the rate constant was found to be independent of UV monitor location (before or after the photolysis cell), linear flow rate through the reaction zone, and the type of photolysis cell. For a total of 61 first-order rate constants at 298 K, the average second-order rate constant ($\pm 2\sigma$) is $1.31 \pm 0.24 \times 10^{-13}$ cm^3 $molecule^{-1}$ s^{-1}. These results and the results at 218, 250, 273, 323, and 363 K are summarized in Table I. An Arrhenius plot

$$k = A \exp(-E/RT) \tag{9}$$

for these results is shown in Fig. 5, and the temperature-dependent rate coefficient is $k_1 = (1.52 \pm 0.43) \times 10^{-14} \exp[(644 \pm 79)/T]$ cm^3 $molecule^{-1}$ s^{-1}. According to gas phase reaction rate theory, a low activation energy E may not be caused by a potential energy barrier between reactants and products, but rather it may simply depend on the net power of T in the rate expression

$$k = BT^n, \tag{10}$$

for which the "activation energy" is nRT. These data are plotted as $\log k$ vs $\log T$ in Fig. 6. The slope indicates the exponent n in Eq. (10) to be -2.29 ± 0.23. Our results are compared with those of other investigators in Table II. The results of this experiment are in very close agreement with those of Wine *et al.*[1] and in reasonably close agreement with those of Kurylo *et al.*[2]

The reaction of HO with H_2O_2

The hydrogen peroxide study covered a sevenfold range of reactant concentration at 298 K and 10 Torr argon

TABLE I. Summary of flash-photolysis/resonance-fluorescence results for the reaction of HO with HNO_3.

Pressure (Torr)	Flow rate in cell[a] (cm s^{-1})	T K	Number of runs	$\frac{k_1 \pm 2\sigma}{10^{-14}}$ (cm^3 s^{-1})	k_1 ave.[b]
10	18	363	9	10.4±1.6	9.6±2.4
25	18		5	9.2±1.2	
10	18	323	5	11.2±2.0	10.6±2.6
25	18		6	10.4±1.3	
10	25[c]	298	21	13.5±1.7	13.1±2.4
10	25[c,d]		6	14.0±2.7	
10	25[c]		4	13.6±2.0	
10	12[c]		4	13.6±3.6	
10	18		6	12.8±1.7	
25	25[c]		8	13.5±1.7	
25	18		6	12.1±1.5	
50	25[c]		6	13.3±1.7	
10	18	273	5	14.8±2.2	15.2±2.6
25	18		5	15.4±1.8	
10	18	250	5	19.3±2.9	19.6±3.2
25	18		5	19.9±2.8	
10	18	218	7	30.8±4.2	30.4±4.6
25	18		5	30.0±3.6	

[a]Flow rate through interaction region.
[b]Error limits cover $\pm 2\sigma$ of all points.
[c]Performed in first cell; other points in cell of Fig. 2.
[d]UV absorption cell placed after photolysis cell; place before cell on other runs.

pressure. Pseudofirst-order rate constants are plotted against H_2O_2 concentrations in Fig. 7. This study covers a tenfold range in initial HO concentration and includes 18 first-order rate constants. The value of the second-order rate constant is $k_2 = (1.81 \pm 0.24) \times 10^{-12}$ cm^3 $molecule^{-1}$ s^{-1}. The result is compared with those of other investigators in Table III. Within the cumulative error limits this result is in agreement with the four recent reports[8-11] that give $k_2 \pm 2\sigma$ of $(1.65 \pm 0.21) \times 10^{-12}$ cm^3 $molecule^{-1}$ s^{-1} at 298 K.

DISCUSSION

The reaction of HO with HNO_3

The rate coefficient for the reaction of hydroxyl radicals with nitric acid has an exceptionally low preexponential factor and a negative activation energy, i.e., the rate constant increases as the temperature decreases. One suggested explanation for these unusual features is that the process is chemically complex, consisting of two or more chemical reactions. The purpose of this section is to see if the results are—after all—quantitatively consistent with transition-state theory as applied to an elementary reaction.

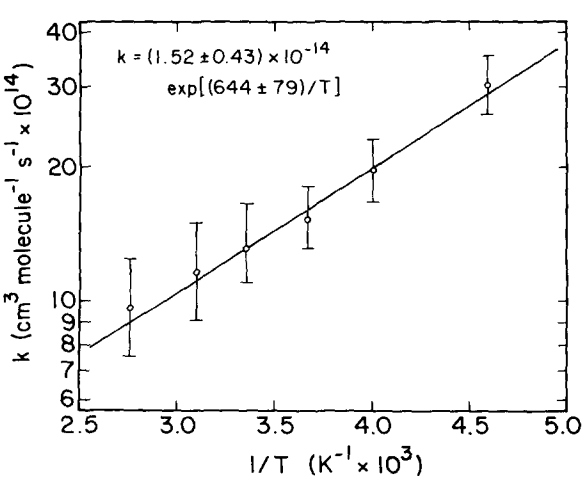

FIG. 5. Arrhenius plot for the reaction of HO with HNO_3 from 218–363 K.

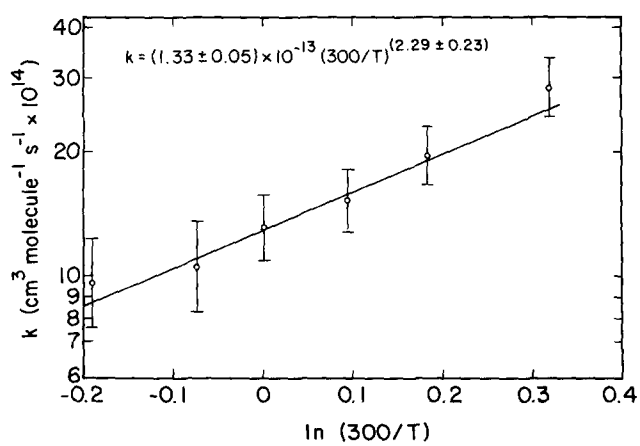

FIG. 6. Test of the temperature expression $k = BT^m$ for the reaction of HO with HNO_3 from 218–363 K.

TABLE II. Summary of kinetic results for the reaction of HO with HNO_3.

Temperature (K)	k_{298}[a] 10^{-13}	A[a] 10^{-14}	E/R[b] (K)	Method[c]	Reference
298	1.7	•••	•••	FP/KS	7
208	1.3	•••	•••	FP/RA	19
230–490	0.90	9.0	0	FP/RA	3
228–472	0.80	8.0	0	FP/RA	4
270–470	0.89	8.9	0	DF/RF	5
298	0.82	•••	•••	FP/RF	6
224–366	1.34	1.52	−649	FP/RF	1
225–300[d]	1.34	1.05	−759	FP/RF	2
218–363	1.32	1.52	−644	FP/RF	This work

[a] cm^3 molecule^{-1} s^{-1}.
[b] $k = A \exp(-E/RT)$.
[c] FP, flash photolysis, KS kinetic absorption spectroscopy, RA resonance absorption, DF discharge flow; RF resonance fluorescence.
[d] The observed points deviated from the Arrhenius function above 300 K.

Nitric acid is a planar molecule, where the hydrogen atom is hydrogen bonded to an oxygen atom to make a four-member ring[20] Fig. 8. The hydrogen atom undergoes an out-of-plane restricted internal rotation with symmetry number two, barrier to rotation of 7 kcal mol^{-1}, and torsional oscillation frequency of about 425 cm^{-1}.[20] The model used for the transition state is included in Fig. 8. The O–H bond in nitric acid is extended by 0.18 Å to become a "half-order" bond,[21] and the new O–H bond being formed is also taken to be a half-order bond. The H–O–H angle is 105°, as in water, and the O–H bond in the approaching hydroxyl radical has the single-bond length of water. The hydrogen atom of the hydroxyl radical is "hydrogen bonded" to an oxygen atom in nitric acid to make a six-membered ring. The N–O bond distances are taken to be the same as in nitric acid. The "reaction coordinate" is the oscillation of the hydrogen atom in the linear O–H–O, half-bonded segment. The potential energy gained by forming the new (1.73 Å) hydrogen bond presumably "pays for" the energy required for the other hydrogen atom to leave nitric acid and become part of the product water molecule.

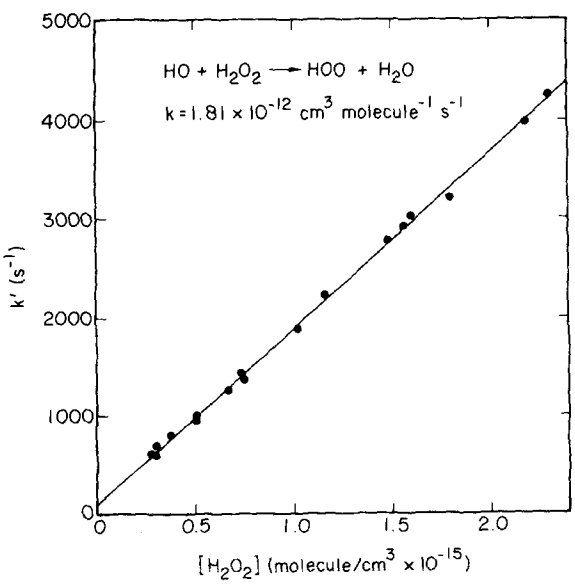

FIG. 7. First-order plot for the reaction of HO with H_2O_2 at 298 K and 10 Torr.

According to transition-state theory,[15] the rate constant is

$$k = \kappa \left(\frac{kT}{h}\right) \frac{q_{\neq}'}{q_A q_B} \exp(-E/T) , \tag{11}$$

where q_A and q_B are molecular partition functions per unit volume, respectively for HNO_3 and HO, $q_{\neq}'$ is the molecular partition function for the transition state omitting the reaction coordinate, κ is the "transmission coefficient" or the probability per vibration of the O–H–O group that the water molecule will form and fly apart, and E is the activation energy in Kelvin units. In standard forms for translational and rotational partition functions, the rate constant may be expressed as

$$k = \kappa \left(\frac{kT}{h}\right) \left(\frac{M_{\neq}}{M_A}\right)^{3/2} \left[\frac{I_1 I_2 I_3 {}_{\neq}}{I_1 I_2 I_3 A}\right]^{1/2} \left(\frac{h^2}{2\pi M_B kT}\right)^{3/2} \times \left(\frac{h^2}{8\pi^2 I_B kT}\right) f(q_v) , \tag{12}$$

where the activation barrier is taken to be zero. The

TABLE III. Summary of kinetic results for the reaction of HO with H_2O_2.

Temperature (K)	k_{298}[a] 10^{-12}	A[a,b] 10^{-12}	E/R[b] (K)	Method[c]	Reference
300–458	0.93	0.41 $T^{1/2}$	604	FP/KS	12
298–670	0.84	7.97	670	DF/ESR	13
298	0.68	•••	•••	FP/RF	14
225–423	1.64	2.51	−126	DF/RF	8
250–459	1.69	2.96	−163	DF/LIF	9
298	1.57	•••	•••	FP/RF	10
273–410	1.57	3.7	−260	FP/RF	11
298	1.81	•••	•••	FP/RF	This work

[a] cm^3 molecule^{-1} s^{-1}.
[b] $k = A \exp(-E/RT)$.
[c] See Table II. Also: ESR electron spin resonance, LIF laser induced fluorescence.

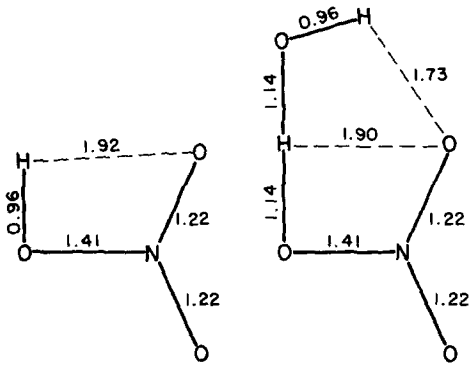

FIG. 8. Structure of nitric acid molecule and the HO · HNO_3 transition state considered in this study.

term $f(q_v)$ involves the vibrational partition functions for reactants and transition state

$$f(q_v) = \prod_{v}^{14} q_{\neq}/q_B \left(q_{ir} \prod_{v}^{8} q\right)_A , \tag{13}$$

where q_{ir} refers to the restricted internal rotation in nitric acid and all other q's have the form

$$q = [1 - \exp(-h\nu/kT)]^{-1} . \tag{14}$$

This model takes the electronic partition function of the transition state to be the same as that for the hydroxyl radical. At the low temperatures of this study, any vibrational frequency greater than about 1000 cm^{-1} has a very small effect on the rate expression, and the key to a simple evaluation of Eq. (12) is to match up and cancel similar terms between the transition state and the reactants and to identify the low frequency terms that do not cancel.

The normal coordinates of nitric acid, hydroxyl radical, and the transition state are classified in Table IV in terms of in-plane (∥) and out-of-plane (⊥) motion, in terms of translational (tr) and rotational (rot) coordinates, and in terms of internal coordinates, including stretching (str), bending (b), internally rotating (i.r.), ring stretching and bending (ring), and reaction (rc) coordinates. In Eq. (12), the translations and rotations of HNO_3 and the transition state are expressed in ratio form, and the corresponding unmatched terms of HO appear in full. Nine vibrational modes are matched in Table IV; most of these have such high frequencies that their partition functions [Eq. (14)] are close to unity at these low temperatures; and even if the partition functions are slightly greater than one, these terms are effectively eliminated by matching and canceling. The unmatched normal coordinates in Table IV are enclosed in parentheses. Aside from the translations and rotations of HO, these unmatched coordinates are the reaction coordinate, the internal rotation of nitric acid, and five vibrations (2 ∥ and 3 ⊥) of the six-membered ring of the transition state. The ratio of vibrational partition functions [Eq. (13)] may be approximately reduced to the form

$$f(q) \sim \prod^{5} (q_v)_{\neq}/(q_{ir})_A . \tag{15}$$

One could assign force constants to the transition state and evaluate the vibration frequencies, but the assignment of force constants is no less arbitrary than assigning vibrational frequencies to the ring motions by analogy to other molecules. Pickett and Strauss[22] evaluated the ring bending frequencies of five molecules with single-bonded six-membered rings: cyclohexane, *s*-trioxane, *p*-dioxane, *m*-dioxane, and tetrahydropyran. The range of values was 229 to 752 cm^{-1}, and the average value was 421 cm^{-1}. The vibrational frequencies of gas-phase formic acid dimers were observed and analyzed.[23–25] These dimers involve a hydrogen-bonded eight-member ring, and identified ring-distortion frequencies were 243, 237, 232, 160, 103, and 60 cm^{-1}. The bonding in the transition state of Fig. 8 is "tighter" than the hydrogen-bonded dimer of formic acid and "looser" than the single-bonded rings in cyclohexane and related compounds. The transition state of Fig. 8 would be expected to have ring motions in the frequency range 100 to 1000 cm^{-1}, the higher end of the range made possible by the low mass of the hydrogen atoms.

The ratio of molecular weights contributes a factor of 1.43 to Eq. (12), the ratio of principal moments of inertia (Fig. 8) contributes a factor of 2.5 to Eq. (12), and the restricted rotor symmetry number is a factor of 2. With the physical and molecular constants and with these ratios, the theoretical rate-constant expression is

$$\frac{k}{cm^3\,s^{-1}} = \left(\frac{3.16\times10^{-10}}{T^{3/2}q_{ir}}\right)(q_{\parallel}^2 q_{\perp}^3)_{\neq} . \tag{16}$$

At low temperatures q_{ir} has the form of Eq. (14) with a torsional frequency of 425 cm^{-1}. As a line of reference, the five frequencies of the transition state were set to very large values (∞); and Eq. (16) was evaluated from 167 to 1000 K and plotted as the dashed curve in Fig. 9, which includes a heavy line based on the observed data. On this simple basis, the calculated rate is slower than that observed, whereas the problem seemed to be too low observed rate constant; and the reaction has a negative activation energy, but less in magnitude than that observed. The five frequencies of the transition state were set equal, assigned values between

TABLE IV. Classification and matching of normal coordinates in the reactants and in the transition state for the reaction HO + HNO_3.

In-plane (∥) motions			Out-of-plane (⊥) motions		
≠	HNO_3	HO	≠	HNO_3	HO
2 tr	2 tr		1 tr	1 tr	
1 rot	1 rot		2 rot	2 rot	
		(2 tr)			(1 tr)
		(1 rot)			(1 rot)
3 NO_3 str	3 NO_3 str		1 NO_3 b	1 NO_3 b	
2 NO_3b	2 NO_3b				
2 H_2O str	1 HO str	1 HO str			
1 H_2O b	1 HON b				
				(1 i.r.)	
(2 ring)			(3 ring)		
(1 r.c.)					
Total: 14	10	4	7	5	2

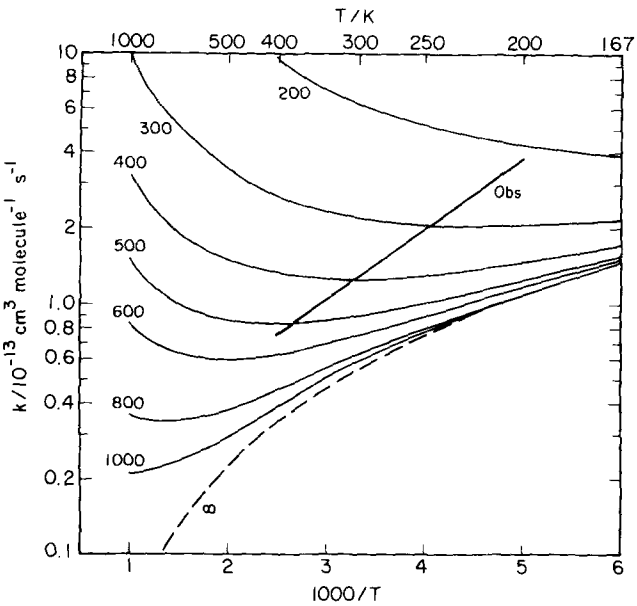

FIG. 9. Comparison of observed and calculated rate constants for Reaction (1) for a range of assigned ring-motion frequencies of the transition state of Fig. 8. The calculated curves are based on Eq. (16), and all five frequencies are assigned the frequencies (cm^{-1}) indicated by the numbers on this figure. For high frequencies, the rate is lower than that observed, and there is a modest negative activation energy. As the assigned frequencies are raised, there is agreement between observed and calculated rate constants at one temperature at a time, but the observed temperature dependence is not matched.

1000 and 200 cm^{-1}, and the rate expression (16) was evaluated between 1000 and 167 K Fig. 9. As the assigned frequencies are decreased, the absolute value of the rate constant increases to give better agreement with observed values, but the temperature dependence moves further away from that observed. At low frequencies, around 200 cm^{-1}, the rate constant increases with increasing temperature. One might expect the hydrogen-atom motions to have higher frequencies than the motions of oxygen and nitrogen atoms. On this basis, two frequencies were set to 1000 cm^{-1} and the other three varied between 800 and 150 cm^{-1}. The fan of calculated curves is similar to that in Fig. 9, and no set of frequencies could be found that more or less matched both the absolute values and the slope (vs T) of the observed rate constants.

Perhaps this discussion should be dropped here, with the assessment that simple transition state theory semiquantitatively accounts for the low pre-exponential factor and some negative activation energy. The discrepancies would then be ascribed to the simplicity of the theory and the crude method of handling the structural model. However, further considerations of the simple theory suggest an additional interpretation.

What is needed to fit the model to the data is a higher power of T in the denominator of Eqs. (12) and (16). The observed power of temperature in the rate expression is -2.29 Fig. 6. The power of temperature in the theoretical expression (16) is -1.5, and any departure of q_v from the low-temperature limit of unity would tend to increase this value. There is no way for Eq. (16) to give a value less than -1.5. However, Eq. (16) may be rewritten as

$$\mathbf{k} = \frac{(\kappa kT/h)\,1.52\times10^{-20}}{T^{5/2}q_{ir}}\,(q_{\parallel}^2 q_{\perp}^3)_{\neq} \tag{17}$$

and one may re-examine the term $(\kappa kT/h)$ in the numerator of Eq. (17).

In the simplest derivation of transition-state theory, the transition state is said to move toward products with a frequency ν^* and this coordinate is ascribed a partition function of the form of Eq. (14). The reaction coordinate is assumed to have a low frequency such that Eq. (14) reduces to the classical-mechanical limit $kT/h\nu^*$,

$$\nu^* q^* = \nu^*[1 - \exp(-h\nu^*/kT)]^{-1} \to kT/h \tag{18}$$

and the unknown frequency of the reaction coordinate cancels to give the universal frequency kT/h. In the present case, the reaction coordinate is the vibration of a hydrogen atom between two oxygen atoms in a six-membered ring. The reaction coordinate is primarily a hydrogen atom motion, and the frequency could be 1000 cm^{-1} or higher. For comparison, the hydrogen stretching motions in a hydrogen bond have frequencies in the range 2500–3500 cm^{-1},[26] but this motion is not strictly comparable to the symmetrically placed hydrogen atom in Fig. 8. Even at 1000 cm^{-1}, the reaction coordinate should be treated by quantum mechanics, not in the sense of quantum mechanical tunneling since there is no activation barrier, but in consideration of the size of one cell in phase space. If ν^* is larger than kT/h, the partition function q^* has the temperature independent value of about one. In this case $\kappa\nu^* q^*$ becomes $\kappa\nu^*$, not $\kappa kT/h$, and with ν^* in units of cm^{-1} the rate expression is

$$\mathbf{k} = \frac{(\kappa\nu^*)\,4.56\times10^{-10}}{T^{5/2}q_{ir}}\,(q_{\parallel}^2 q_{\perp}^3)_{\neq}\,. \tag{19}$$

Another derivation of transition-state theory involves a distance δ, across which one calculates the reaction frequency $p/m\delta$; and the classical partition function is δ/Λ where Λ is the Boltzmann average de Broglie wavelength $h/(2\pi mkT)^{1/2}$. This component of rate is integrated over the classical-mechanical Boltzmann distribution of momentum and over the reaction coordinate for the distance δ to produce the expression kT/h. Since in this problem there is no potential energy barrier, one may assign δ an unusually large value, say 0.1 Å, compare Fig. 8. In this case at room temperature, the Uncertainty-Principle momentum for a hydrogen atom corresponds to a zero-point energy along the reaction coordinate that exceeds kT by a factor of 8, whereas it should be much less than kT to justify the continuous integrations that are carried out. Even along the constant potential-energy channel, the reaction coordinate involves an almost temperature-independent quantum-mechanical frequency factor related to zero-point energy.

The rate constant $\mathbf{k}$ was evaluated from Eq. (19) using several sets of transition-state frequencies as adjustable parameters. For values of $\nu_{\parallel}$ and $\nu_{\perp}$ used in Fig. 9 and

in other similar calculations, the value of ($\kappa\nu^*$) was adjusted to give $k = 9.0\times10^{-14}$ cm^3 s^{-1} at 400 K, and then the effect of temperature from 400 to 200 K was predicted. This procedure is illustrated for eight sets of frequencies in Table V and in Fig. 10. The upper panel in Fig. 10 includes the observed points by Wine *et al.*[1] and this study, the lower panel gives only the observations in this study. All eight of these sets of frequencies give satisfactory agreement between theory and experiment. The values of ($\kappa\nu^*$) range between 244 and 551 cm^{-1}. The best agreement with experiment comes from values of the ring frequencies: 1000 (twice) and about 450 (three times), or alternatively by about 550 cm^{-1} (five times). These frequencies are within the range of those observed in single-bonded six-membered rings[22] and are somewhat higher than those observed in a hydrogen-bonded eight-member ring.[23–25] Although the value of κ is indeterminate in this analysis, the value of $\kappa\nu^*$ is within the expected range, especially if κ is 0.5 or somewhat less. The ring-deformation frequencies fitted here to the activated complex are somewhat higher than expected.

It is well to recall alternative physical explanations to the language of transition state theory. The partition functions do not represent time averages over one collision, but rather are ensemble averages.[15] The meaning of the tightly bound six-membered ring is that the molecule HNO_3 and the radical HO must collide in a constrained solid angle so that the potential energy gained by the transient intermolecular hydrogen bond compensates for a potential energy barrier in other parts of the collision complex. The limited volume of phase space for these constrained angles of approach is expressed in other words as a ring structure.

It is not claimed that this model and these vibration frequencies represent the transition-state-theory solution to the rate of this reaction. Rather this theoretical study indicates that it may not be necessary to postulate a complex mechanism for this reaction. The simple transition-state method, modified to have a quantum-mechanical reaction coordinate, is capable of explaining the magnitude and the temperature dependence of this rate in terms of a tight cyclic transition state, whose frequencies are marginally within the range of those expected.

TABLE V. Parameters adjusted to obtain the calculated curves in Fig. 10, k(400 K) adjusted to give $\kappa\nu^*$.

$\nu(\parallel)$ (cm^{-1})	$\nu(\perp)$ (cm^{-1})	$\kappa\nu^*$ (cm^{-1})
1000	600	482
1000	500	404
1000	400	310
1000	350	256
800	800	551
600	600	399
500	500	299
450	450	244

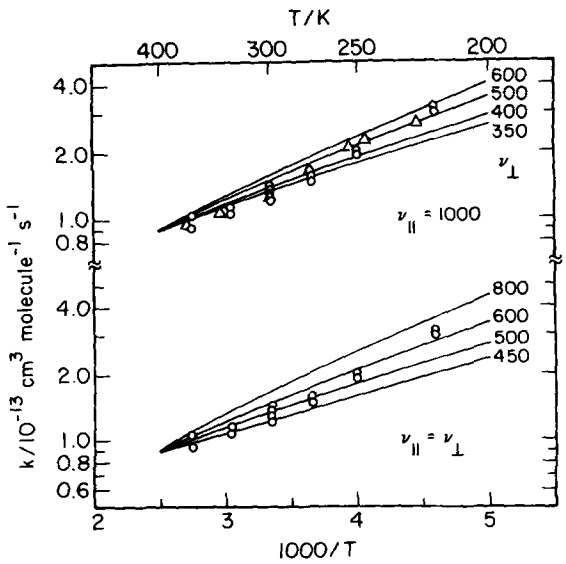

FIG. 10. Calculated curves and observed rate constants: triangles Ref. 1, circles, this work. The curves are calculated by means of Eq. (19). The five "new" frequencies of the transition state are the numbers given (cm^{-1}) taken five times for the lower panel; three equal frequencies are assigned the numbers given in the upper panel and the other two are assigned 1000 cm^{-1}. In each case, ($\kappa\nu^*$) of Eq. (19) is adjusted to give agreement between theory and experiment at 400 K; these values are listed in Table V.

The reaction of HO with H_2O_2

At 298 K the rate constant for Eq. (2) is 12 times that for Eq. (1), and the ratio of pre-exponential factors A_2/A_1 is 165. If the discussion above gives a semi-quantitative account of the low value of k_1 and of its increase with decreasing temperature, one should use the same language to compare Reaction (2) to Reaction (1). The model of the transition state of Reaction (2) is taken to be a zig–zag six-membered chain, with a linear O $\cdots$ H $\cdots$ O segment. Such a structure would have two internal rotation coordinates. In comparing k_2 and k_1, all reference to the hydroxyl radical cancels out, the ratio of molecular weights and moments of inertia [compare Eq. (12)] are not greatly different for the two cases, and similar frequencies can be cancelled between transition state and reactant (HNO_3 or H_2O_2). To a reasonable approximation, the ratio of rate constants is

$$\frac{k_2}{k_1} = \frac{(q_{ir})_A}{(q_{ir})_P}\,\frac{(q_{ir}^2 q_v^3)_{\neq P}}{(q_v^5)_{\neq A}} \approx \frac{(q_{ir})^2_{\neq P}}{(q_v)^2_{\neq A}}\ , \qquad (20)$$

where A refers to nitric acid and P refers to peroxide. The vibration frequencies of the ring structure in the transition state for Eq. (1) were assigned values of about 400 cm, for which the value of the partition function is about 1.2 at 298 K. If the reduced moment of inertia for the internal rotation of the transition state in Eq. (2) is taken to be 1×10^{-40} g cm^2 (the value of the lowest principal moment of inertia in H_2O), the partition function for free internal rotation is about five at 298 K. The square of 5/1.2 is 17, and thus Eq. (20) indicates that k_2 could easily exceed k_1 by the observed factor of 12 at 298 K.

The "free internal rotations of the transition state" of Reaction (2) can also be expressed in other words.

As the oxygen atom of the hydroxyl radical approaches a hydrogen atom of H_2O_2, a large solid angle of approach leads to reaction, and for each satisfactory line of this approach the orientation of the hydrogen atom on the hydroxyl radical can take on 2π values about the third Euler angle χ_r. This situation is to be contrasted with Reaction (1) where both O and H in HO must hit an H and O in HNO_3 in a constrained manner. Transition-state theory provides a simple method to demonstrate that this difference is large enought to account for the differences observed in the rates of Reactions (1) and (2).

ACKNOWLEDGMENT

This work was supported by the Director, Office of Energy Research, Office of Basic Energy Sciences, Chemical Sciences Division of the U.S. Department of Energy under Contract No. DE-AC03-76SF00098.

[1]P. H. Wine, A. R. Ravishankara, N. M. Kreutter, R. C. Shah, J. M. Nicovich, R. L. Thompson, and D. J. Wuebbles, J. Geophys. Res. **86**, 1105 (1981).
[2]M. J. Kurylo, K. D. Cornett, and J. L. Murphy, J. Geophys. Res. (to be published).
[3]R. Zellner and I. W. M. Smith, Chem. Phys. Lett. **26**, 72 (1974).
[4]I. W. M. Smith and R. Zellner, Int. J. Chem. Kinet. Symp. **1**, 341 (1975).
[5]J. J. Margitan, F. Kaufman, and J. G. Anderson, Int. J. Chem. Kinet. Symp. **1**, 281 (1975).
[6]H. H. Nelson, W. J. Marinelli, and H. S. Johnston, Chem. Phys. Lett. **78**, 495 (1981).
[7]D. Husain and R. G. W. Norrish, Proc. R. Soc. London Ser. A **273**, 165 (1963).
[8]L. F. Keyser, J. Phys. Chem. **84**, 1659 (1980).
[9]U. C. Sridharan, B. Reimann, and F. Kaufman, J. Chem. Phys. **73**, 1286 (1980).
[10]H. H. Nelson, Ph.D. thesis, University of California, Berkeley, and Lawrence Berkeley Laboratory Report LBL-11666, 1980.
[11]P. H. Wine, D. H. Semmes, and A. R. Ravishankara, J. Chem. Phys. **75**, 4390 (1981).
[12]N. R. Greiner, J. Phys. Chem. **72**, 406 (1968).
[13]W. Hack, K. Hoyermann, and H. G. Wagner, Int. J. Chem. Kinet. Symp. **1**, 329 (1975).
[14]G. W. Harris and J. N. Pitts, J. Chem. Phys. **70**, 2581 (1979).
[15]H. S. Johnston, *Gas Phase Reaction Rate Theory* (Ronald, New York, 1966).
[16]F. Magnotta, Ph.D. thesis, University of California, Berkeley, and Lawrence Berkeley Laboratory Report LBL-9981, 1979.
[17]P. H. Wine, N. M. Kreutter, and A. R. Ravishankara, J. Phys. Chem. **83**, 3191 (1979).
[18]L. T. Molina and M. J. Molina, J. Photochem. **15**, 97 (1981).
[19]C. Morley and I. W. M. Smith, J. Chem. Soc. Faraday Trans. 2 **68**, 1016 (1972).
[20]W. R. Forsythe and W. F. Giauque, J. Am. Chem. Soc. **64**, 529 (1942).
[21]L. Pauling, *The Nature of the Chemical Bond*, 3rd ed. (Cornell, Ithaca, 1960), p. 255.
[22]H. M. Pickett and H. L. Strauss, J. Chem. Phys. **53**, 376 (1970).
[23]R. C. Milliken, Ph.D. thesis, University of California, Berkeley, 1957.
[24]T. Miyazawa and K. S. Pitzer, J. Am. Chem. Soc. **81**, 74 (1959).
[25]L. Bonner and J. S. K. Smith, Phys. Rev. **57**, 1078 (1940).
[26]G. C. Pimentel and A. L. McClellan, *The Hydrogen Bond* (Freeman, San Francisco, 1960), p. 68.